



# TROPESS-CrIS CO single-pixel vertical profiles: intercomparisons with MOPITT and model simulations for 2020 western US wildfires

Ming Luo<sup>1</sup>, Helen M. Worden<sup>2</sup>, Robert D. Field<sup>3,4</sup>, Kostas Tsigaridis<sup>3,5</sup>, and Gregory S. Elsaesser<sup>3,4</sup>

<sup>1</sup>Jet Propulsion Laboratory, California Institute of Technology, Pasadena, CA 91109, USA

<sup>2</sup>National Center for Atmospheric Research, 1850 Table Mesa Dr, Boulder, CO 80305, USA

<sup>3</sup>NASA Goddard Institute for Space Studies, 2880 Broadway, New York, NY 10025, USA

<sup>4</sup>Department of Applied Physics and Applied Mathematics, Columbia University, 2880 Broadway, New York, NY 10025, USA

<sup>5</sup>Center for Climate Systems Research, Columbia University, 2880 Broadway, New York, NY 10025, USA

**Correspondence:** Ming Luo (ming.luo@jpl.nasa.gov)

Received: 23 June 2023 – Discussion started: 15 September 2023

Revised: 6 February 2024 – Accepted: 28 February 2024 – Published: 6 May 2024

**Abstract.** The new TROPESS (TROpospheric Ozone and its Precursors from Earth System Sounding) profile retrievals of carbon monoxide (CO) from the Cross-track Infrared Sounder (CrIS) are evaluated against Measurement of Pollution in the Troposphere (MOPITT) CO version 9 data. Comparison results that were adjusted to common a priori constraints in the retrieval processes have improved agreement between the two data sets over direct comparisons. TROPESS-CrIS CO profiles are within 5% of MOPITT but have higher concentrations in the lower troposphere and lower concentrations in the upper troposphere. For the intense western US wildfire events in September 2020, we compare CO fields simulated by the GISS climate model to the two satellite CO observations. We show intermediate steps of the comparison process to illustrate the evaluation of model simulations by deriving the “retrieved” model CO profiles as they would be observed by the satellite. This includes the application of satellite level-2 data along with their corresponding diagnostic operators provided in the TROPESS-CrIS and MOPITT products. The process allows a diagnosis of potential model improvements in modeling fire emissions and pollution transport.

## 1 Introduction

As a direct pollutant to Earth’s atmosphere, carbon monoxide (CO) is a product of incomplete combustion which has a lifetime of weeks to months. CO has therefore been used as a tracer in atmospheric ozone-related photochemistry and pollution transport studies. High concentrations of CO in source regions can be seen above background concentrations from, for example, biomass burning, traffic, and other fossil fuel combustion in polluted cities and industrial areas (Jacob, 1999). High-CO plumes are seen extending downwind to pollute nearby regions and sometimes circling the globe. For more than 20 years, retrievals of vertical CO profiles or total columns based on satellite measurements of CO absorption bands of 4.7 and 2.3  $\mu\text{m}$  have been made available from several platforms, such as the Measurement of Pollution in the Troposphere (MOPITT) (Drummond et al., 2009), Atmospheric Infrared Sounder (AIRS) (Aumann et al., 2003), Tropospheric Emission Spectrometer (TES) (Beer et al., 2001), Infrared Atmospheric Sounding Interferometer (IASI) (Clerbaux et al., 2009), Cross-track Infrared Sounder (CrIS) (Han et al., 2013), and TROPOspheric Monitoring Instrument (TROPOMI) (Veefkind et al., 2012). In addition, some limited CO data also became available, e.g., from GOSAT (Noël et al., 2022) and GIIRS (Zeng et al., 2023) satellite observations. These satellite CO observations are valuable in tracking and quantifying pollutant emissions, horizontal gradients in pollution patterns, and the pollutant photochemical processes occurring as air moves (Clerbaux et al., 2002). From

a long-term and global point of view, the satellite CO observations have been used to track the pollution–time trend in geophysical regions annually and seasonally (Worden et al., 2013; Buchholz et al., 2021). The satellite CO observations have also been used to evaluate parameter variations that drive model simulations of the atmospheric system (Field et al., 2015, 2016; Buchholz et al., 2018).

In this paper, we focus on (1) satellite-retrieved profile comparisons between the newly available CrIS CO from Tropospheric Ozone and its Precursors from Earth System Sounding (TROPES) (Bowman, 2021; Worden et al., 2022), which uses the MUSES (Multi-SpEctra, Multi-SpEcies, Multi-Sensors of Retrievals of Trace Gases) algorithm (Fu et al., 2016) and the MOPITT V9 data (Deeter et al., 2022), and (2) comparisons of TROPES-CrIS and MOPITT CO to the NASA Goddard Institute for Space Studies (GISS) model simulations for September 2020 wildfire events in the western US. We present some details in understanding the a priori constraints used by different instrument retrieval algorithms and their influences in the final retrieval products. We illustrate how the measurement and retrieval characteristics provided in the data products should be used in data applications, such as model evaluation processes aimed at improving some parameters important in model development.

## 2 Satellite CO observations: TROPES-CrIS and MOPITT comparison

### 2.1 CO retrievals from two satellite observations

The observation configurations of the CrIS instrument on NOAA S-NPP and NO-20 and the MOPITT instrument on NASA Terra satellites are listed in Table 1. The spectral sensitive ranges of both instruments cover carbon monoxide absorption bands in thermal infrared (TIR); MOPITT also covers the CO absorption band in near-IR. For the CrIS and MOPITT comparison studies in this paper, we do not consider the MOPITT data products using NIR or TIR/NIR-combined CO retrievals.

CrIS is an infrared Fourier transform spectrometer on board the NOAA Suomi- National Polar-orbiting Partnership (Suomi-NPP) and the Joint Polar Satellite System-1 (JPSS-1 or NOAA-20) satellite operating since 2011 and 2017, respectively ([https://www.jpss.noaa.gov/mission\\_and\\_instruments.html](https://www.jpss.noaa.gov/mission_and_instruments.html), last access: 22 April 2024, and <https://www.star.nesdis.noaa.gov/jpss/CrIS.php>, last access: 22 April 2024). Its sun-synchronous orbits cover the entire globe with 16 d local footprint repeat time. Under the TROPES project, the MUSES data processing system (Fu et al., 2016) inherited from the TES project is running forward in time, providing CrIS CO and other atmospheric gas retrievals at a reduced global sampling – one every 0.8° latitude and longitude box. SNPP/CrIS makes measurements at

local early afternoon (13:30 local time, LT) and after midnight hours. Each CrIS pixel or field of view (FOV) is circular with a 14 km radius at nadir. The TROPES-CrIS CO products use single-pixel radiances with the MUSES algorithm (Fu et al., 2016, 2018, 2019) that applies an optimal estimation retrieval approach (Rodgers, 2000) with heritage from Aura/TES (Tropospheric Emission Spectrometer) level-2 processing (Bowman et al., 2006). The TROPES retrieval approach and TROPES-CrIS CO products differ from other available CrIS CO products that combine nine FOVs to obtain a single cloud-cleared radiance and corresponding retrieval of atmospheric parameters such as the NOAA Unique Combined Atmospheric Processing System (NUCAPS) (Gambacorta and Barnet, 2013; Gambacorta et al., 2014) and the Community Long-term Infrared Microwave Combined Atmospheric Product System (CLIMCAPS) (Smith and Barnet, 2020). MOPITT is a satellite gas filter correlation radiometer (GFCR) instrument that has been operating on NASA Terra since 1999 with over 23 years of data (<https://www2.acom.ucar.edu/mopitt>, last access: 22 April 2024). The onboard gas absorption cells and radiometers are used to derive CO concentrations in the atmosphere similar to a high spectral resolution spectrometer (Drummond et al., 2010). Terra orbits also repeat every 16 d, and MOPITT obtains global coverage in ~ 3 d. However, MOPITT observation local times are 10:30 and 22:30 LT, different from that of SNPP/CrIS. The MOPITT FOV is 22 km × 22 km.

### 2.2 The comparisons between CO retrievals from the two satellite observations

Here we compare MOPITT and TROPES-CrIS CO vertical profile retrievals from MOPITT V9T data (version 9, thermal infrared only) and the TROPES Release 1.12 data. Both MOPITT and TROPES-CrIS CO retrievals have been validated against aircraft in situ and other satellite measurements (George et al., 2009, 2015; Luo et al., 2007a, b; Deeter et al., 2019; Hegarty et al., 2022; Worden et al., 2022). Although the two data sets demonstrate general agreement in global distribution patterns in the lower, middle, and upper troposphere, such as variation between source regions, land vs. ocean, and the seasonality in the two hemispheres, there are some local differences mainly due to different observation times and locations. To provide context for comparison differences we examined CO volume mixing ratio variabilities in MOPITT data. For example, within a 500 km area and 24 h of a typical day in September, CO variations are about 12 % and 15 % in the lower and upper troposphere in North America, respectively.

The CO vertical profile retrievals from both MOPITT and TROPES-CrIS are based on optimal estimation theory (Rodgers, 2000). The estimated radiance noise levels of the satellite instruments are propagated to retrieval measurement error (or precision). The a priori knowledge about the

**Table 1.** Observation configurations for CrIS and MOPITT.

	Launch time	Orbit nadir local time	Swath width	Footprint size at nadir	Instrument type and spectral range for CO retrieval	Daily no. of pixel scan observations
CrIS	S-NPP (since October 2011) NOAA-20 (since November 2017)	S-NPP 01:30 and 13:30 NOAA-20 02:20 and 14:20	2200 km	14 × 14 km	Fourier transform spectrometer (TIR 2160–2200 cm <sup>-1</sup> )	~ 3.5 million
MOPITT	NASA-Terra (since December 1999)	10:30 and 22:30	650 km	22 × 22 km	Gas filter correlation radiometer (TIR 2140–2195 cm <sup>-1</sup> )	300 000

horizontal and vertical distributions from a CO climatology are also important constraints in the optimal estimate process. The a priori CO profiles are used as initial-guess profiles for both TROPES and MOPITT CO retrievals. Different data processing teams use different a priori data. This will therefore cause differences in their retrieved profiles and the accompanying characteristic data. The steps for comparing TES-MOPITT CO profiles, i.e., how these are adjusted for the different a priori data, have been presented in Luo et al. (2007b). We selected a few days of TROPES and MOPITT data over the four seasons of 2016 and made inter-satellite CO retrieval comparisons following the steps referenced above. The statistical comparison conclusions (details not shown) are similar for the selected days. They are also similar to a specific example case we show below.

Figure 1 shows coincident pairs of MOPITT and TROPES-CrIS CO volume mixing ratios (VMRs) at the pressure level of 681 hPa for 12 September 2020. The lower troposphere 681 hPa is one of the forward model pressure levels used in TROPES-CrIS retrievals defined via 12 levels between 1000 and 100 hPa uniformly in log(pressure). We apply coincidence criteria so that the retrievals are within 24 h and 500 km of each other. TROPES-CrIS CO concentrations are higher over eastern China and the biomass burning region of southern Africa and lower over the western US, but otherwise there is general agreement in global CO distribution patterns.

MOPITT processing (V7 and later) uses a climatology from CAM-Chem (Lamarque et al., 2012; Tilmes et al., 2016) for the spatial and seasonal (but not interannual) variability in the CO a priori profiles. This is somewhat different from the MOZART climatology (Brasseur et al., 1998) used in the TROPES algorithm. Both MOPITT and TROPES-CrIS use the same vertical constraint (a priori covariance) of 30 % uncertainty for CO parameters at all levels and a correlation length of 100 hPa between them in the troposphere. The use of the same prior covariance simplifies the intercomparison of satellite products (George et al., 2015).

Figure 2 shows the CO a priori VMRs ( $x_a$ ) at 681 hPa for 12 September 2020 for the two instrument retrievals. From the MOZART model field, the TROPES algorithm derives the monthly means over 10° latitude × 60° longitude blocks

to extract CO a priori profiles for CrIS; MOPITT interpolates the CAM-Chem model field (with 1.9° latitude × 2.5° longitude) at the observation location and time. The different climatology sources and how they are applied spatially results in many differences in  $x_a$  when comparing coincident pairs. For example, as we show later, the  $x_a$  used in MOPITT and TROPES-CrIS retrievals are very different in magnitude for this day in the western US when several large wildfires occurred.

As described and illustrated in Worden et al. (2007) and Luo et al. (2007b), the trace gas profile retrievals are strongly influenced by the a priori data, especially for the nadir-viewing satellite instruments. For CO profile retrievals the degrees of freedom for signal (DOFS) are generally less than 2. This means the profiles only have a couple of independent information points vertically. The following equation describes the relationship between a retrieved CO profile ( $x_{\text{retv}}$ ) and the unknown “true profile” ( $x_{\text{true}}$ ) assuming the known initial climatology state ( $x_a$ ) is close to its “truth” with the uncertainty constraint (the linearization is valid):

$$x_{\text{retv}} = \mathbf{A}x_{\text{true}} + (\mathbf{I} - \mathbf{A})x_a + e, \quad (1)$$

where  $\mathbf{A}$  is the averaging kernel matrix describing the sensitivity of the retrieved state to the true state, and  $e$  is the error mainly due to instrument measurement noise. The averaging kernel is determined by the sensitivity of the measurement to the retrieved CO state (Jacobian matrix) and the prior covariance matrix used to constrain the retrieved profile with only a couple of vertical degrees of freedom for signal (DOFS). The detailed linear retrieval estimate equation and the definition equations for  $\mathbf{A}$  can be found in Rodgers (2000). We examine the DOFS of the two instrument CO retrievals for September 2020 (Fig. 1). The DOFS for TROPES-CrIS CO is larger than that of MOPITT CO by 0.1–0.2 (their global averaged DOFS are 1–2), indicating a slightly higher vertical resolution in TROPES-CrIS CO retrieved profiles.

Since TROPES-CrIS retrievals use the a priori CO profiles derived from a similar atmospheric model and the same constraints as MOPITT products, we can directly compare the retrieval products of the two data sets with relatively good agreement. For example, the global total CO column comparisons between TROPES-CrIS and MOPITT shown in Fig. 3

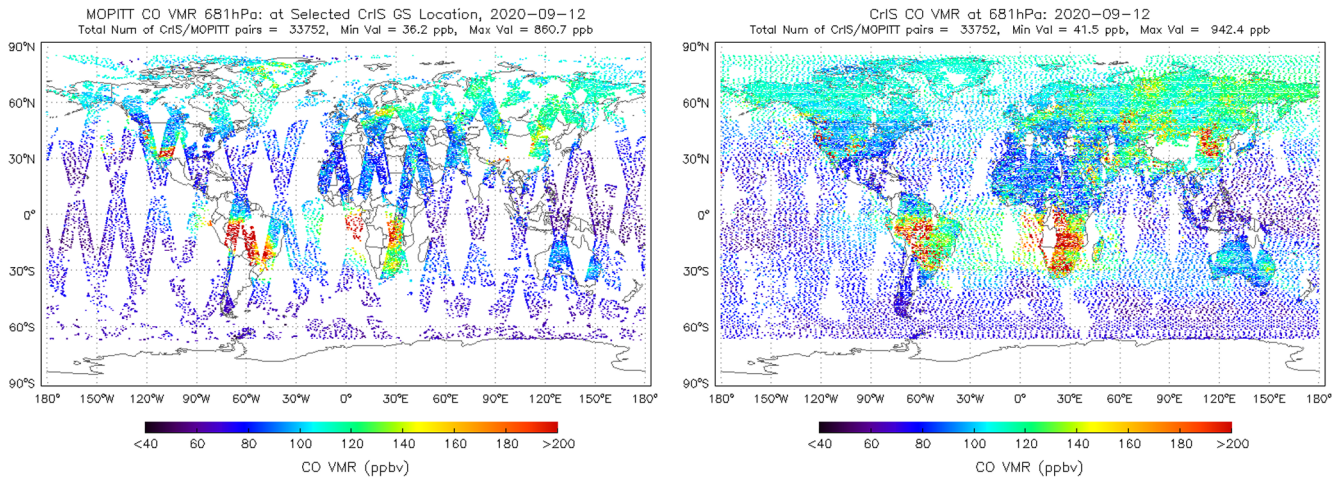


**Figure 1.** MOPITT and TROPES-CrIS CO profiles matched in location (within 500 km) and time (24 h). MOPITT CO profiles are mapped to TROPES-CrIS standard pressure levels. The CO volume mixing ratio (VMR, in ppbv) corresponding to 681 hPa is shown for 12 September 2020. The footprints are enlarged for illustration.

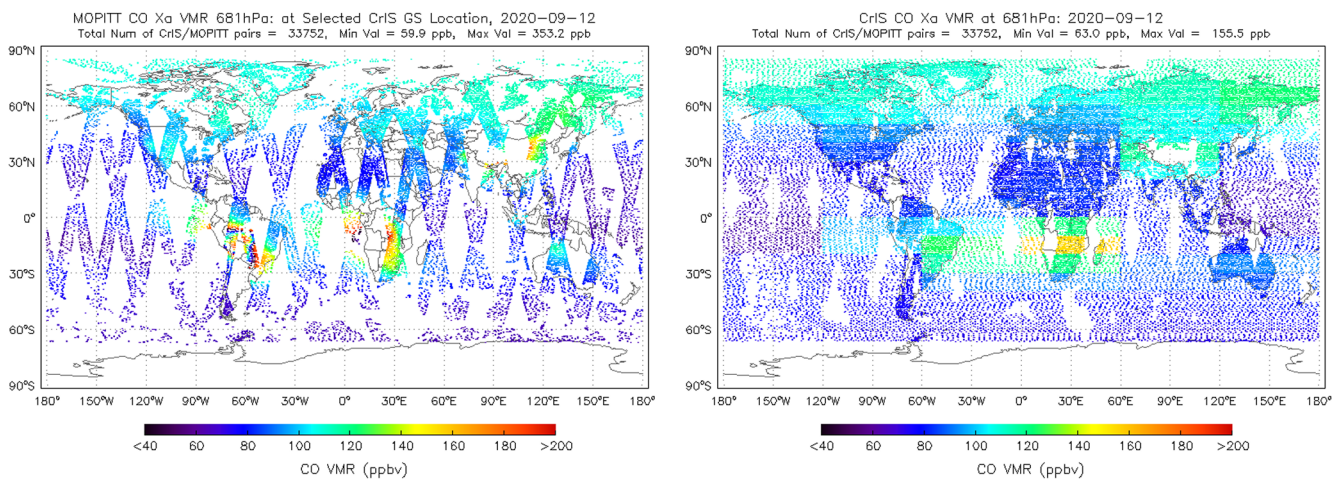


**Figure 2.** The a priori CO profile VMRs at 681 hPa used in MOPITT and TROPES-CrIS CO retrievals 12 September 2020, respectively. See the text for climatology descriptions. MOPITT data use interpolation to observation local time and location while TROPES-CrIS applies monthly means over latitude–longitude blocks to determine the a priori profiles.

agree very well in the zonal mean. However, the vertical integration of the CO profile to obtain total columns can average out potential disagreements in vertical sub-layers.

We present comparisons of TROPES-CrIS and MOPITT CO profiles at different pressure levels. We follow the procedure and equations described in Luo et al. (2007b) for making direct comparisons by adjusting the MOPITT a priori profile  $x_a$  to that of CrIS and smoothing the CrIS profiles with the MOPITT averaging kernel (A). The smoothing procedure is applied to TROPES-CrIS CO profiles because their DOFS, e.g., zonally averaged, are slightly larger than that of MOPITT. As we emphasized, the influences of the different a priori data used in the profile retrievals will contribute to the disagreement of the trace gas profile products provided by different retrieval teams. Examples of the results

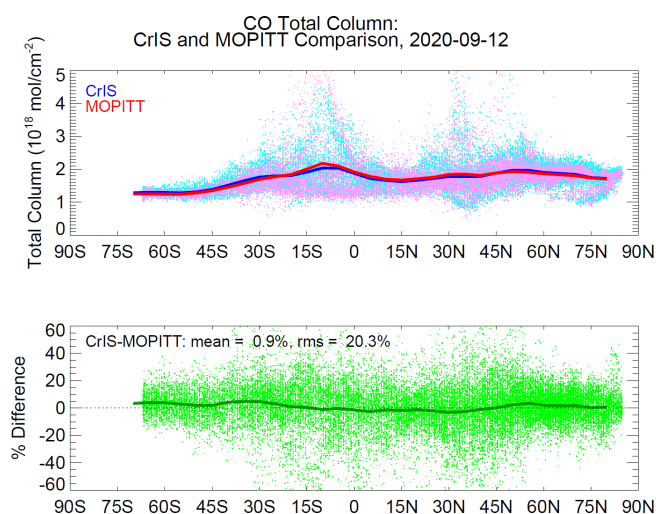
are shown in Fig. 4 at 681 and 215 hPa. Table 2 summarizes the comparison statistics for 12 September 2020.

Each step in the comparison process reduced disagreement between TROPES-CrIS and MOPITT CO, as expected. At 681 hPa, their direct globally averaged difference was 6.7 % (CrIS minus MOPITT) with 35 % rms; this difference was reduced to 6 % with 27 % rms with the a priori adjustment, and further reduced to 5.1 % with 23 % rms with the application of the averaging kernel. At 215 hPa, the three-step comparisons are  $-11\%$  (33 % rms),  $-4.7\%$  (31 % rms), and  $-3.8\%$  (23 % rms). We also listed the percent retrieval error (Retv Err %) and precision (Retv Precision %). The above-quoted mean differences are comparable to the retrieval precisions and within the CO natural variability of 12 %–15 % mentioned above.

**Table 2.** TROPES-CrIS and MOPITT CO comparison summary, 12 September 2020.

		A priori $x_a$	Direct comp	Adj $x_a$	Adj $x_a$ and AK	Retv err %		Retv precision %	
						CrIS	MOP	CrIS	MOP
Total column	% Diff					10 %	8.6 %		
	% rms								
681 hPa	% Diff	−1 %	6.7 %	6 %	5.1 %	25 %	12 %	4.6 %	2 %
	% rms	23 %	35 %	27 %	23 %				
215 hPa	% Diff	−10.8 %	−11.4 %	−4.7 %	−3.8 %	25 %	12 %	6 %	3 %
	% rms	9.7 %	33 %	31 %	23 %				

Note that Diff refers to TROPES-CrIS – MOPITT CO, while rms refers to the root mean square of the difference.

**Figure 3.** Comparisons of CrIS and MOPITT CO total column retrievals, 12 September 2020.

We note that even after adjusted two data sets for the slight differences in the a priori assumptions, compared to MOPITT, TROPES-CrIS CO VMRs are still  $\sim 5\%$  higher in the lower troposphere and  $\sim 4\%$  lower in the upper troposphere. This result is in good agreement with previous work comparing satellite CO profiles to in situ observations (Luo et al., 2007a; Hegarty et al., 2022; Deeter et al., 2022; Worden et al., 2022).

### 3 Comparisons of model CO simulations to the satellite CO retrievals

The above analyses of the two satellite CO profile retrieval comparisons have shown that satellite data users should not treat retrieved data products as the “truth”. The retrieval characteristic data, e.g., the a priori profiles and the averaging kernels derived from the retrieval processes are key parameters in the applications. Here we briefly describe the GISS

Earth system model (ModelE2) as an example in this study. In the next two sections, we illustrate the proper use of the retrieval data sets in model evaluations.

#### 3.1 GISS Earth system model

The GISS ModelE2 simulates the interactions between the different components of the Earth system. The model can be used to study a wide range of climate phenomena, including the impacts of greenhouse gases, aerosols, and other atmospheric pollutants on the climate. We used the NASA GISS-E2 version described in Kelley et al. (2020), with prescribed sea surface temperatures and interactive chemistry. Aerosols are coupled to the tropospheric chemistry scheme which includes inorganic chemistry of  $O_x$ ,  $NO_x$ ,  $HO_x$ , and CO and organic chemistry of  $CH_4$  and higher hydrocarbons.

Anthropogenic fluxes come from the Community Emissions Data System inventory (Hoesly et al., 2018) and sea salt, dimethyl sulfide, isoprene, and dust emission fluxes are calculated interactively. All other forcings, such as solar, volcanic (prescribed as stratospheric aerosol optical depth (AOD) and aerosol size), and land use follow the CMIP6 protocol (Eyring et al., 2016). Biomass burning emissions and injection heights are prescribed from the Global Fire Assimilation System (GFAS) (Kaiser et al., 2012; Rémy et al., 2017) at a daily time step, rather than monthly averages and boundary layer distribution of fire emissions used in base CMIP6 configuration. Emission sources in September 2020 mainly due to the intense wildfires in western US and the background biomass emissions. These are shown for CO in Fig. 5 for 12 September 2020, for both the original GFAS  $0.1^\circ \times 0.1^\circ$  resolution and the ModelE2  $2.0^\circ \times 2.5^\circ$  resolution, obtained by re-binning from the higher-resolution GFAS grid to the coarse ModelE2 grid while conserving total emissions. The CO emission hot spots are associated with the reported wildfires in the news, such as the Bobcat fire in Angeles National Forest and the Creek Fire in the Sierra National Forest ([https://en.wikipedia.org/wiki/2020\\_California\\_wildfires](https://en.wikipedia.org/wiki/2020_California_wildfires), last ac-

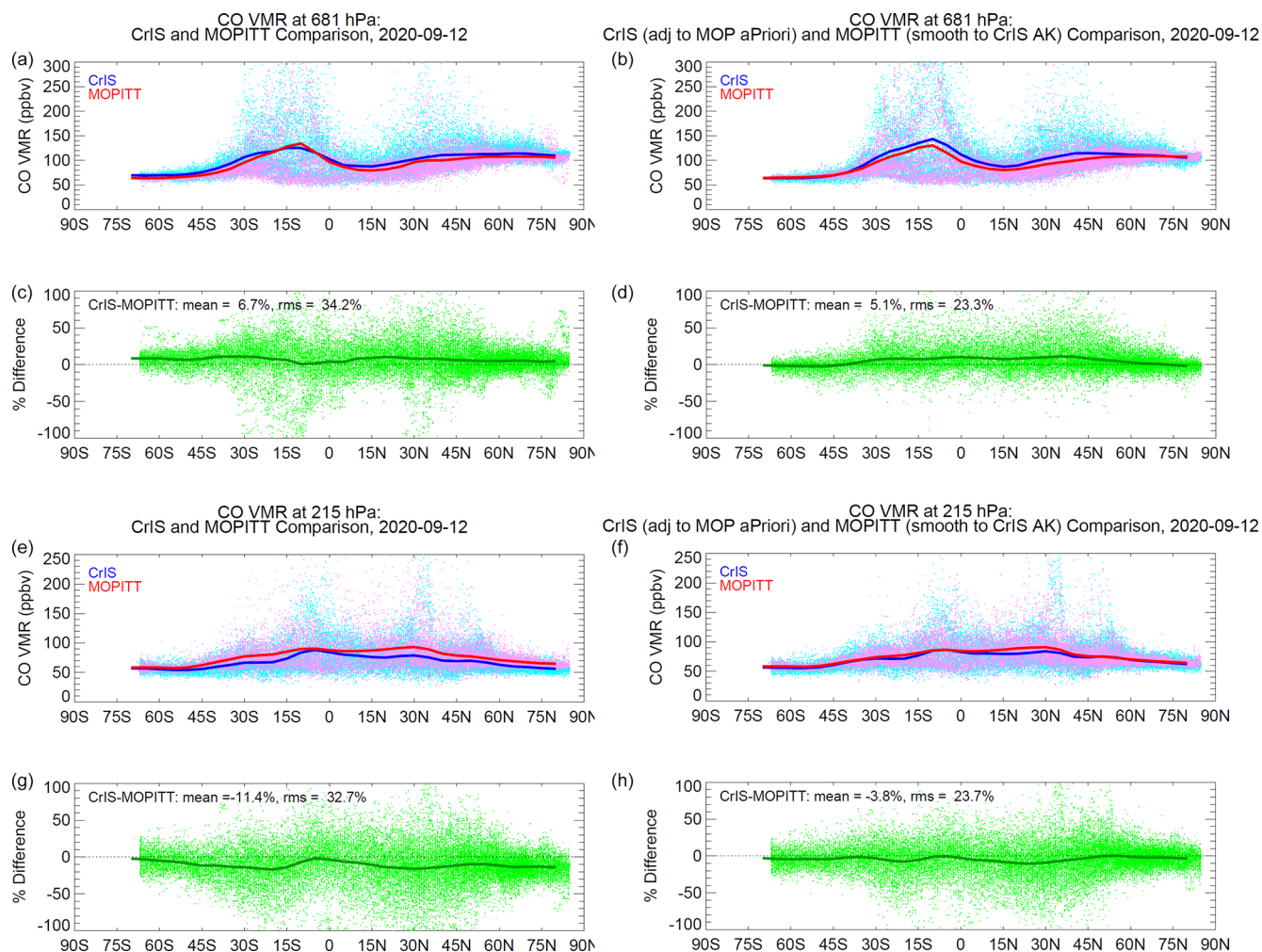


**Figure 4.** TROPES-CrIS and MOPITT CO comparisons at 681 hPa (a–d) and 215 hPa (e–h), 12 September 2020. The left column shows the direct comparisons, and the right column show the comparison of CrIS adjusted to MOPITT a priori profile Xa and MOPITT smoothed by the CrIS averaging kernel.

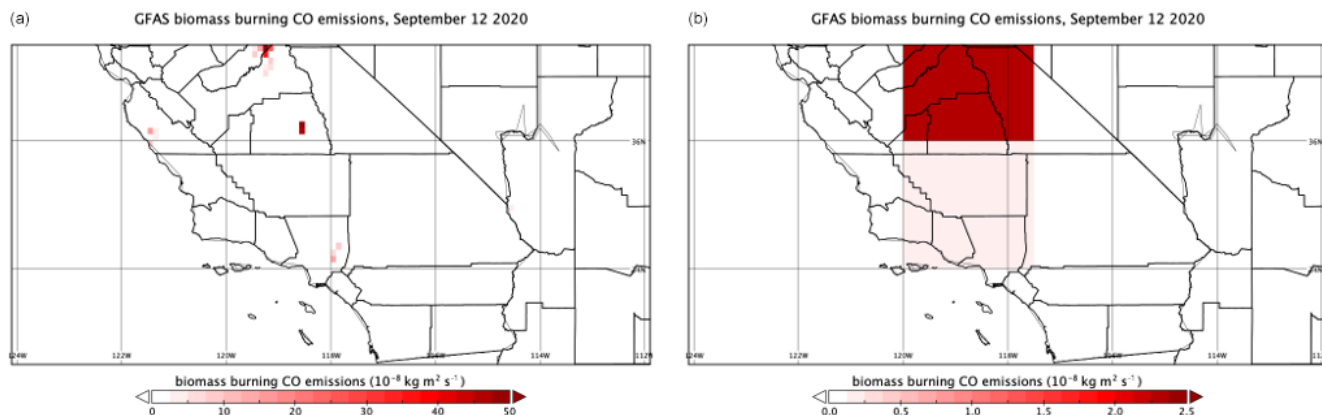


**Figure 5.** CO emission sources on 12 September 2020. (a) The wildfire flux of CO in the Global Fire Assimilation System (GFAS) source files at  $0.1 \times 0.1^\circ$  latitude–longitude. (b) The same GFAS CO emissions converted to ModelE2 input at  $2 \times 2.5^\circ$  latitude–longitude, noting the different scale.

cess: 22 April 2024). Several large wildfires also occurred in the states of Oregon and Washington ([https://en.wikipedia.org/wiki/2020\\_Western\\_United\\_States\\_wildfire\\_season](https://en.wikipedia.org/wiki/2020_Western_United_States_wildfire_season), last access: 22 April 2024).

Time evolution of the distributions of enhanced CO due to fires depends on emission fluxes and the transport processes in the atmosphere. We nudged GISS ModelE2 horizontal winds to National Centers for Environmental Prediction (NCEP) reanalysis (Kalnay et al., 1996), driving the trace gas transport away from the fire source areas. Some model parameters that determine the gas initial locations, such as the injection heights over fires and the aerosol scheme, are subjects of model parameter evaluations using in situ and remote observations. We leave these detailed ModelE2 investigations to another publication by Field et al. (2023). The CO model output used in this paper are at  $2^\circ \times 2.5^\circ$  latitude by longitude and hourly intervals. They were sampled at the geolocations and times of satellite profile retrievals for comparisons.

### 3.2 Proper comparisons of model to the satellite CO retrievals

Here we use CO data during the western US wildfires in September 2020 to illustrate the steps of comparing GISS ModelE2 CO simulations to CrIS and MOPITT CO observations. This follows other model–satellite comparisons with biomass burning as a key CO source for a single wildfire event (Field et al., 2016) and at seasonal (Liu et al., 2010; Field et al., 2015) and interannual scales (Strode et al., 2016), for example.

As we described in Sect. 2, TROPES-CrIS and MOPITT provide CO profile retrievals with DOFS of 1–2 over clear-sky conditions. Figure 6 shows CO VMR distributions from TROPES-CrIS and MOPITT observations taken on 12 September 2020 over the US in the middle troposphere at about 450 hPa. This vertical range is the sensitivity peak of the satellite nadir observations to the CO local concentrations. TROPES-CrIS and MOPITT CO maps show very good agreement in highlighting the huge CO plumes that originated from the catastrophic wildfires (e.g., <https://www.nasa.gov/centers-and-facilities/jpl/nasa-monitors-carbon-monoxide-from-california-wildfires/>, last access: 22 April 2024). In Fig. 7, we also show the satellite CO maps near the surface at 750 hPa where the outstanding high CO VMRs are most likely closer to the emission sources – the burning area at the ground over land. Over the ocean, the high CO values are mostly due to the combination of tracer transport from its origin and the effect of vertical smoothing in retrievals.

There are some noticeable differences in CO distributions at two pressure levels (Figs. 6 and 7). For example, the high CO over the Pacific Ocean in TROPES-CrIS maps is less apparent in MOPITT distributions. In addition to the maximum value of 24 h in time and the exact footprint differences

(comparing the dot maps in Fig. 1 over the western US), the instrument noise contributing to the retrieval errors is a factor too. The precision (measurement error due to noise in spectral radiances) and the total retrieval error for TROPES-CrIS (Bowman et al., 2006) are over twice of that for MOPITT (Table 2). One of the reasons is perhaps that the MOPITT retrievals are flagged as missing due to the thick smoke (Deeter et al., 2022).

The ModelE2 CO field at  $2 \times 2.5$  latitude–longitude grid and 1 h time interval described in Sect. 3 are sampled at the satellite observation locations and times. The next step is to calculate the “retrieved profile” assuming the model profile is the “truth” following Eq. (1). This retrieved profile obtained via applying retrieval operator is the proper way of comparing the model to the satellite data retrievals.

In ModelE2-CrIS CO comparisons, the left panels of Fig. 8 show the model “raw” CO maps with model time–location sampling at SNPP/CrIS observations. In the right panels of Fig. 8, the model-retrieved CO maps, described above for 12 September 2020 at pressures of 464.2 and 749.9 hPa, respectively, are shown. At the pressure level near the surface (749 hPa or about 2.5 km), the CO emission source distributions and the near-surface transport effects are seen in the model simulations. The model raw CO distributions exhibit strong CO emissions from multiple wildfire sources in the western US. It also demonstrated fire plume transport patterns similar to the CO maps of TROPES-CrIS and MOPITT, e.g., a spiraling segment to the Pacific Ocean and a separate eastward segment (Fig. 7). It appears that the model meteorological winds near the surface effectively transport the fire-generated pollutants over long distances. These model features are mostly confined to 749.9 hPa, with an isolated enhancement at 464.2 hPa of up to  $\sim 170$  ppbv only over the US Midwest. The proper model–satellite CO concentration comparison is to compare the retrieved model CO (right panels in Fig. 8) with CrIS CO at the same pressure levels (Figs. 6 and 7). At 464.2 hPa, the model CO feature is still apparent after applying the TROPES-CrIS retrieval operator but less pronounced than the raw CO, peaking at  $\sim 150$  ppbv. Closer to the surface at 749.9 hPa, the effect of the retrieval operator is greater, with most of the enhanced model CO absent except for an isolated feature over the Pacific Northwest. These comparisons illustrate the relatively low sensitivities in satellite profile retrievals, especially near the surface, and their effect on the raw model profiles. The smoke injection heights prescribed from GFAS were also likely to be underestimated given the intensity of the fires leading up to 12 September 2020 (Lassman et al., 2023).

Similarly, the model–MOPITT CO comparisons shown in Fig. 9 show almost the same conclusions as model to TROPES-CrIS CO comparisons. In addition to the CO distribution patterns at two pressure levels that we discussed above, the differences in model raw map and the model-retrieved map after using the satellite retrieval operator is obvious, especially in lower troposphere (749.9 hPa), although

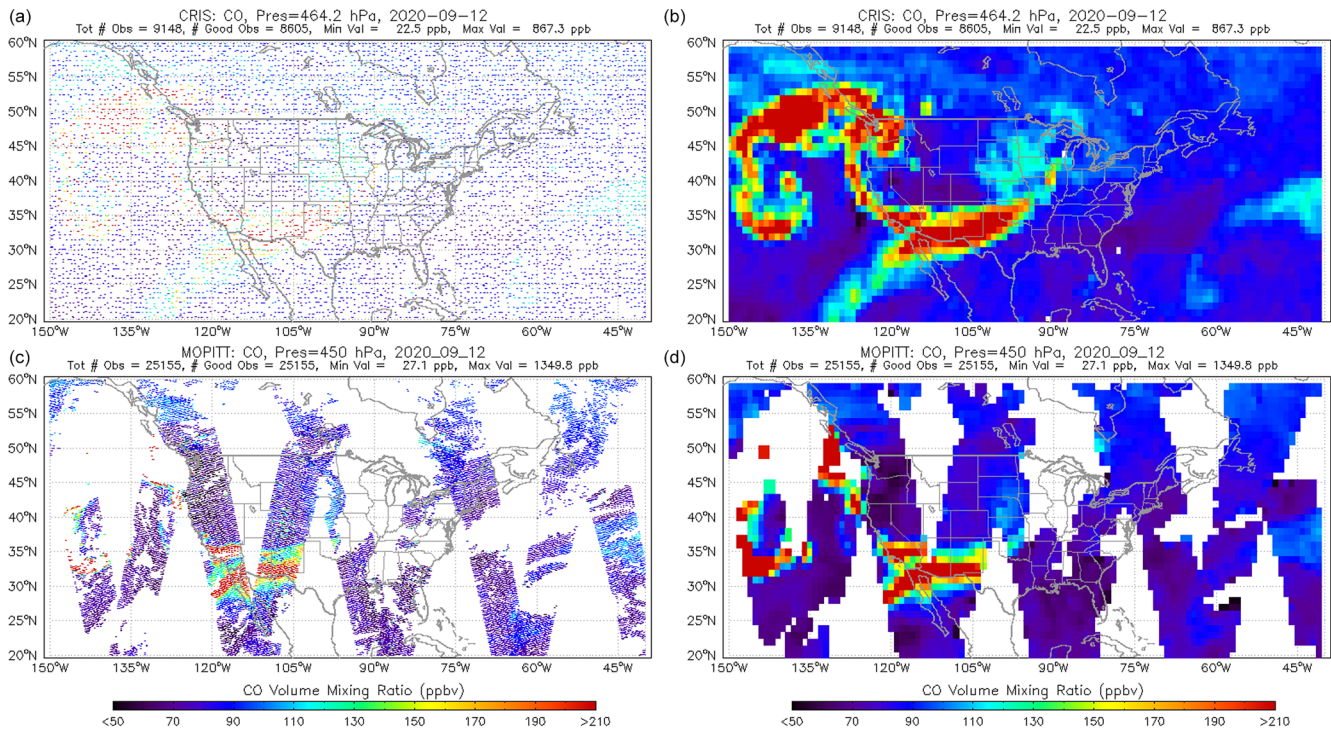


**Figure 6.** The CO value colored dots (a, c) at observation locations and  $1 \times 1^\circ$  latitude–longitude averaged (b, d) CO VMR maps at 464.2 hPa for TROPES-CrIS (a, b) and 450 hPa for MOPITT (c, d).

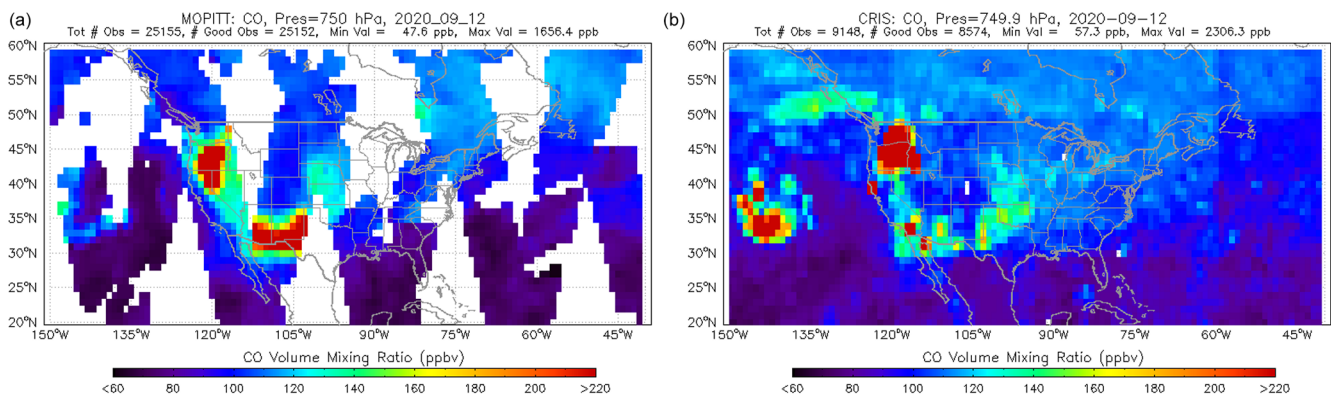


**Figure 7.** The  $1 \times 1^\circ$  latitude–longitude-averaged CO VMR maps at 750 hPa for MOPITT (a) and 749.9 hPa for TROPES-CrIS (b).

there the model CO enhancement remains more apparent compared to the TROPES-CrIS to retrieved model CO possibly because of MOPITT's slightly greater retrieval sensitivity near the surface. As we reference the satellite data a priori CO VMRs shown in Fig. 2, we know in the lower troposphere that the influence of the a priori data on the retrieved profiles is very large (the second term of Eq. 1). In the next section, we use the averaging kernels of an example profile to demonstrate this influence.

#### 4 Discussion of model–satellite profile comparisons

Equation (1) in Sect. 2 presents a simple relationship between the true species profile and the retrieved one. It assumes that the initial guess of the profile in the iterative optimal retrieval process is close to the climatology mean (the a priori  $x_a$ ) described by the a priori constraint matrix defining the variability of the mean. For a given spectral radiance satellite measurement, a different a priori profile could result in a different retrieved profile even if using the same constraint matrix. Note that the a priori values (also used as the initial-guess profiles) are chosen differently for the two project teams in

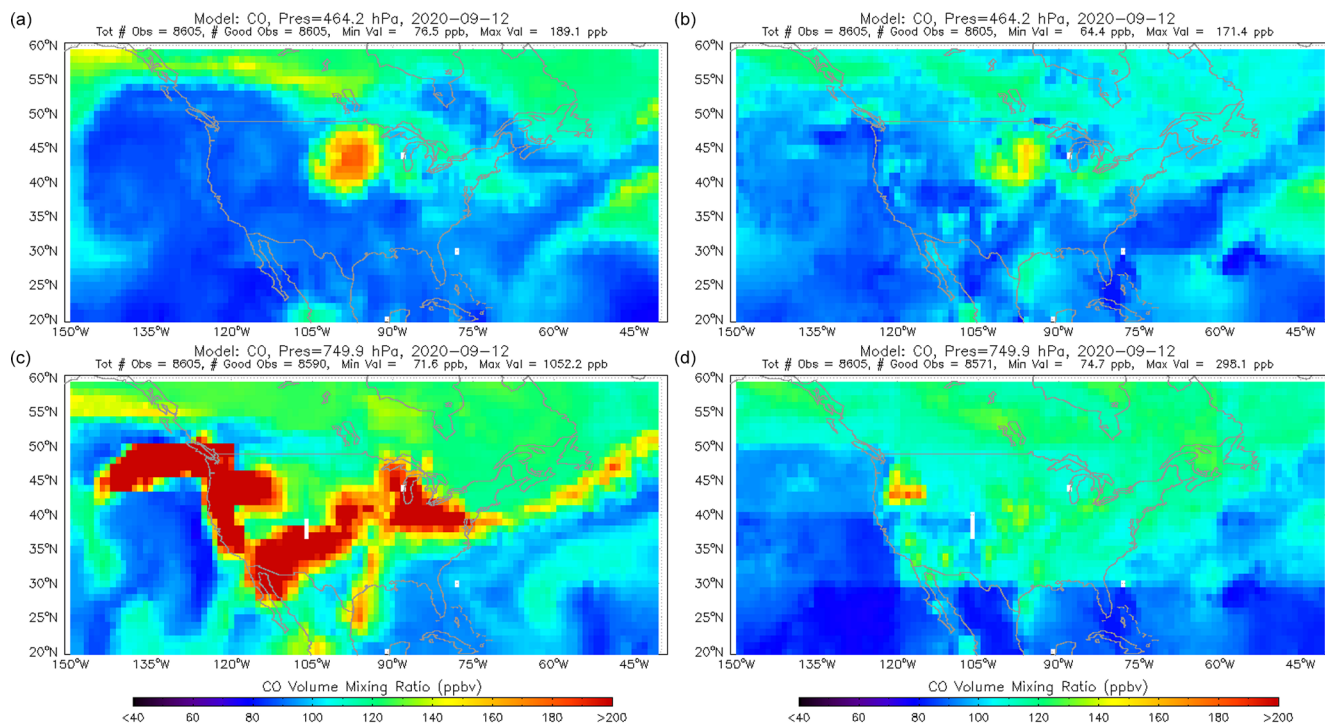


**Figure 8.** GISS model CO VMRs for 12 September 2020 at 464 hPa (a, b) and 749.9 hPa (c, d). Model CO profiles are sampled at SNPP/CrIS time and footprints and averaged at  $1 \times 1^\circ$  latitude–longitude grids (a, c). Panels (b) and (d) show the “retrieved” model CO profiles from their “raw” data using TROPES-CrIS retrieval operator (Eq. 1).

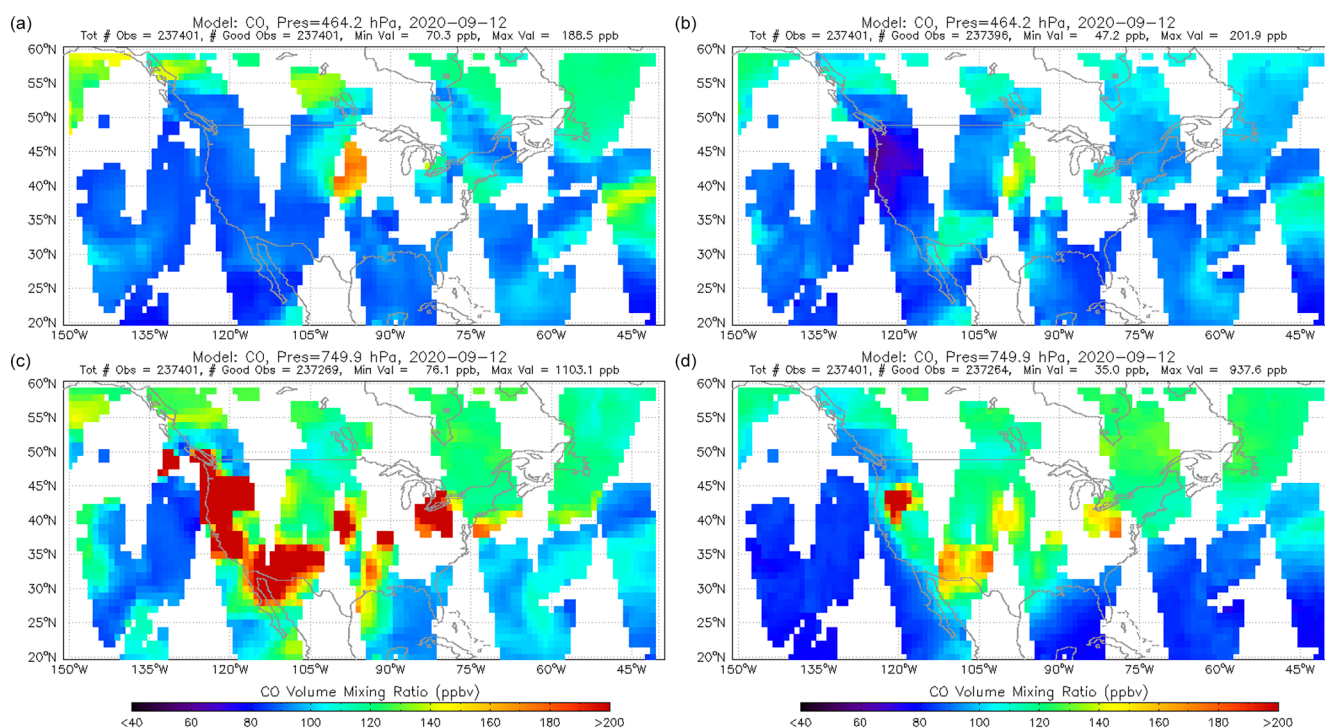


**Figure 9.** Similar to Fig. 8 but showing the GISS model-MOPITT sampling and retrieval operator application.

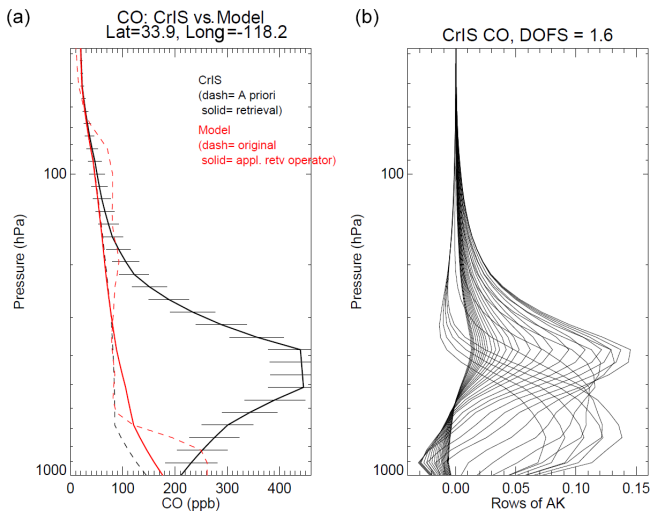


**Figure 10.** CO profile comparisons at  $34.2^{\circ}\text{N}$ ,  $118^{\circ}\text{W}$  on 12 September 2020 near the Bobcat fire center. Panel (a) shows (1) TROPES-CrIS CO retrieved with error bars and the a priori (dash) profiles in black and (2) the matched original model CO profile (dashed red) and the “model-retrieved” profile after applying CrIS retrieval operator (solid red). Panel (b) shows the CrIS averaging kernels.

TROPES-CrIS and the MOPITT CO retrievals (Fig. 2). We use one fire scenario to discuss the details.

From the CO fire maps in Figs. 6–9, 12 September 2020, we selected one CO enhancement in southern California that is common to the CrIS and MOPITT data. This is likely influenced by emissions from the Bobcat fire near Mt. Wilson observatory burning in a large foothill area (<https://earthobservatory.nasa.gov/images/147324/bobcat-fire-scorches-southern-california>, last access: 22 April 2024). Using the fire center at  $34.2^{\circ}\text{N}$ ,  $118^{\circ}\text{W}$ , we identified one profile each from TROPES-CrIS and MOPITT observations. We use the criteria of the observation location that was among the closest to the fire and had the maximum DOFS in CO retrievals. Due mainly to the remaining mismatch in location and time near the fires, TROPES-CrIS CO values are  $\sim 2 \times$  the MOPITT CO values in the mid-troposphere.

Figure 10 shows the selected CrIS and the matched model CO profile comparison. Figure 11 shows the selected MOPITT and its matched model CO profile comparison. In these comparison cases, both TROPES-CrIS and MOPITT profiles show very high CO in the mid-troposphere (700–300 hPa), while neither the original or the retrieved model profiles display any CO enhancement at these higher altitudes. Since the satellite AK peaks are in these mid-troposphere levels, the model retrievals are only moderately increased compared to the original one, indicating the very weak CO plume transports vertically or a weaker CO emission in model setup near the surface.

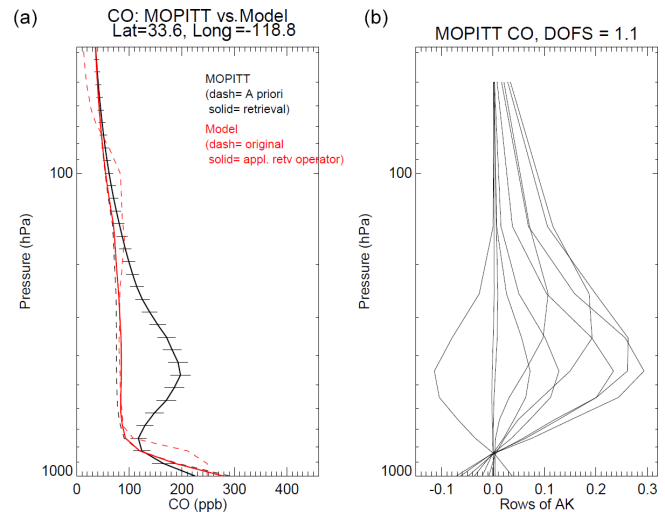


**Figure 11.** Similar to Fig. 10, but showing the satellite CO profile from MOPITT.

Near the surface, according to the averaging kernels of the two instruments, the satellite-retrieved CO profiles should be insensitive to the CO emissions. The retrieved profiles were therefore pulled over to the values of the a priori profiles. We also noted that the a priori guess of TROPES-CrIS and MOPITT CO were different due to the different ways that the two teams used to derive them (Sect. 2) – TROPES-CrIS and MOPITT CO surface a priori values are less and greater than 200 ppb, respectively, for the case discussed here. The retrieved model CO values near the surface are therefore pulled to the a priori profiles (the solid red lines in Figs. 10 and 11). These changes in the model CO maps are also seen in the right panels of Figs. 8 and 9.

We also examined total column comparisons between the corresponding model and satellite profiles in Figs. 10 and 11. Model CO total column ( $2.4 \times 10^{18} \text{ mol cm}^{-2}$ ) underestimated column CO values retrieved by the TROPES-CrIS ( $5 \times 10^{18} \text{ mol cm}^{-2}$ ) and MOPITT ( $3 \times 10^{18} \text{ mol cm}^{-2}$ ).

Figure 12 shows the result of using the MOPITT CO a priori profile near the Bobcat fire as the initial guess and a priori (dashed black line, Fig. 11) in the collocated CrIS CO profile. Compared to the CrIS retrieval using the TROPES  $x_a$  (Fig. 10), the retrieval using the MOPITT  $x_a$  resulted in a different CO profile, especially near the surface. This is due to dominant contributions from the a priori profile near the surface where the averaging kernels have lower sensitivity to the true profile. Based on the results of Kulawik et al. (2008), due to nonlinearities in the retrieval process we do not expect full retrievals of profiles that assume an a priori to match exactly with retrievals where that same prior is “swapped” in a single step following the retrieval iterations (the method described in Sect. 2) with a different a priori.

Figure 13 shows comparisons of CrIS CO profiles generated via three retrieval configurations. In the left panel, two

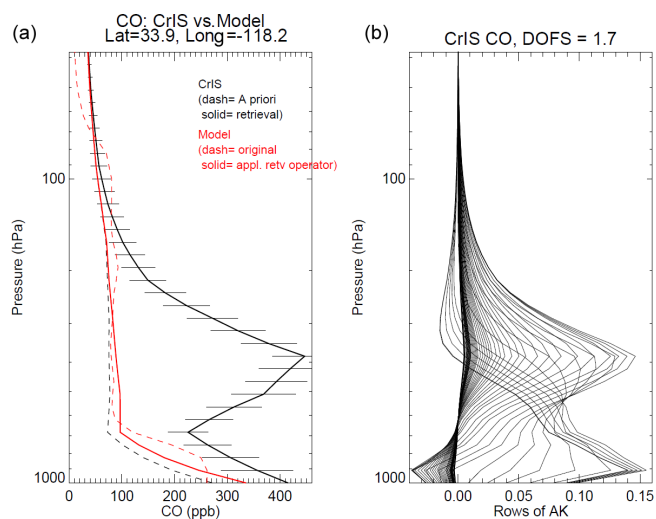


**Figure 12.** In panel (a), the CrIS CO retrieved profile is generated from MOPITT a priori, which is also used as the initial guess (black); the “model-retrieved” profile (solid red) is derived using this new TROPES-CrIS retrieval operator. Panel (b) shows the corresponding TROPES-CrIS CO averaging kernel for this new retrieval.

dashed lines show the different a priori and initial-guess profiles from the TROPES and MOPITT algorithms. The corresponding CrIS CO retrievals are shown in solid black and red profiles. At 700–300 hPa, compared to the two very similar a priori profiles, we see strongly enhanced CO layers in both retrievals, indicating the dominant observable signal from fire-enhanced CO in the mid-troposphere and lower troposphere. Near the surface we see the dominant effect of the a priori profile in the retrieved CO values.

The third way to derive a retrieved CO profile is via swapping the a priori  $x_a$ . The blue profile in the left panel of Fig. 13 is obtained by simply adjusting the TROPES-CrIS CO a priori from the original retrieval to that of MOPITT (Luo et al., 2007b). This profile (blue) is very similar to the full retrieved CO profile (red); however, differences remain, as shown in the right panel of Fig. 13. As found in Kulawik et al. (2008), the profile differences from these two approaches are small and are due to retrieval nonlinearities. These profile differences can be evaluated using the retrieval precision due to instrument noise terms (a few percent, as listed in Table 2), which demonstrates the validity of the simpler approach (i.e., swapping the a priori value) before comparing profiles from different instruments or retrievals.

## 5 Summary

The TROPES algorithm including the a priori assumptions inherited from the TES project has been used to retrieve several atmospheric species profiles from CrIS and other satellite nadir spectral measurements. Here we made the com-

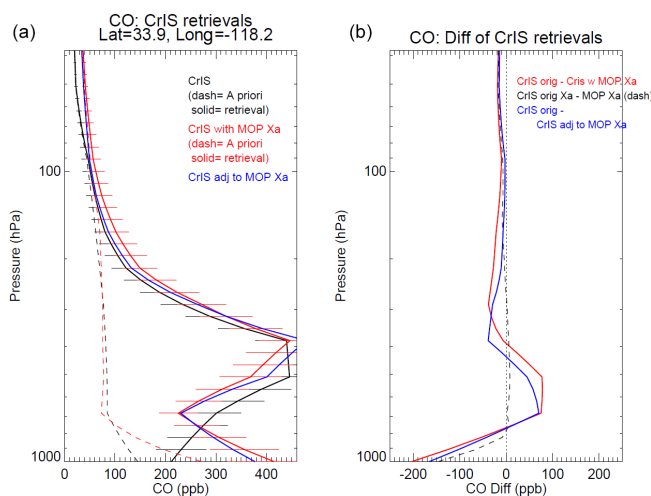


**Figure 13.** Panel (a) shows the overlaid CrIS CO retrieved and the a priori profile (black), CrIS CO retrieved using the MOPITT a priori profile (red), and the CrIS CO adjusted with the MOPITT a priori profile using Eq. (1) (blue). Panel (b) shows their comparisons, CrIS CO retrieval minus CrIS CO retrieval using MOPITT a priori (red), CrIS a priori  $X_a$  minus MOPITT  $X_a$  (dashed), and CrIS CO retrieval minus CrIS CO adjusted to MOPITT X (blue).

parisons of TROPES-CrIS and MOPITT CO retrieved profiles globally in steps of adjusting their a priori and vertical smoothing effects. A better agreement between the two satellite data sets is achieved at the last step. The slight biases of TROPES-CrIS CO compared to MOPITT are about 5% in the lower troposphere and –3% in the upper troposphere. The rms of the above bias is 23%, which can mostly be explained by the CO 12%–15% variabilities in 24 h and 500 km area, and the measurement errors of 2%–6% of the two instruments are due to their radiance measurement noises.

Using the GISS ModelE2, we illustrated the proper method for making model–satellite CO profile retrieval comparisons, a necessary step in evaluating model-crucial parameters. For data taken during the historical large wildfires in the western US in September 2020, the retrieval a priori dominates near the surface where the satellite measurements have less sensitivity causing the model-retrieved CO to move toward the a priori. In the mid-troposphere where TROPES-CrIS and MOPITT show the maximum sensitivity to the true concentrations in their retrievals, the model retrieval departs from the satellite retrievals. This disagreement indicates unmatched CO emission locations and times and (or) yet to be improved tracer transport schemes in GISS model, particularly in the vertical direction. We use the CO vertical profiles near the Bobcat fire center to examine this model–satellite comparison situation.

Finally, the TROPES-CrIS and MOPITT single CO profile retrievals are used to illustrate the comparison of adjusting to a common a priori for the retrievals mathematically vs.

carrying out the retrievals end to end. We found that swapping the a priori mathematically works well.

**Data availability.** TROPES-CrIS CO products are available via the GES DISC from the NASA Tropospheric Ozone and its Precursors from Earth System Sounding (TROPES) project at <https://doi.org/10.5067/EA7G2TTV84RV> (Bowman, 2021). The MOPITT version 9 products are available from NASA through the EARTHDATA portal (<https://doi.org/10.5067/TERRA/MOPITT/MOP02T.009>, NASA/LARC/SD/ASDC, 2024).

**Author contributions.** ML planned and carried out the study. ML and HMW discussed and wrote the manuscript components regarding the TROPES and MOPITT CO comparisons. RDF and KT provided GISS ModelE2 results, description, and analyses. RDF, KT, and GSE contributed to discussions about model–satellite comparisons. RDF edited the manuscript. All authors reviewed the manuscript.

**Competing interests.** At least one of the (co-)authors is a member of the editorial board of *Atmospheric Measurement Techniques*. The peer-review process was guided by an independent editor, and the authors also have no other competing interests to declare.

**Disclaimer.** Publisher's note: Copernicus Publications remains neutral with regard to jurisdictional claims made in the text, published maps, institutional affiliations, or any other geographical representation in this paper. While Copernicus Publications makes every effort to include appropriate place names, the final responsibility lies with the authors.

**Acknowledgements.** We would like to thank the TROPES science and software teams for their algorithm insights, supportive discussions, and data processing. We especially thank Susan Kulawik for the discussions about retrieval algorithms and Valentin Kantchev for setting up the MUSES processing code.

**Financial support.** Part of this research was carried out at the Jet Propulsion Laboratory, California Institute of Technology, under contract with the National Aeronautics and Space Administration via the Tropospheric Ozone and its Precursors from Earth System Sounding (TROPES) project. The project is also supported by NASA grant no. 80NSSC18K0166.

**Review statement.** This paper was edited by Thomas Wagner and reviewed by three anonymous referees.

## References

- Aumann H. H., Chahine, M. T., Gautier, C., Goldberg, M. D., Kalnay, E., McMillin L. M., Revercomb, H., Rosenkranz, P. W., Smith, W. L., Staelin, D. H., Strow, L. L., and Susskind, J.: AIRS/AMSU/HSB on the Aqua mission: design, science objectives, data products, and processing systems, *IEEE T. Geosci. Remote*, 41, 253–264, <https://doi.org/10.1109/TGRS.2002.808356>, 2003.
- Beer, R., Glavich, T. A., and Rider, D. M.: Tropospheric emission spectrometer for the Earth Observing System's Aura satellite, *Appl. Optics*, 40, 2356–2367, 2001.
- Bowman, K. W.: TROPES CrIS-SNPP L2 Carbon Monoxide for Forward Stream, Standard Product V1, Greenbelt, MD, USA, Goddard Earth Sciences Data and Information Services Center (GES DISC) [data set], <https://doi.org/10.5067/EA7G2TTV84RV>, 2021.
- Bowman, K. W., Rodgers, C. D., Kulawik, S. S., Worden, J., Sarkissian, E., Osterman, G., Steck, T., Lou, M., Eldering, A., Shephard, M., Worden, H., Lampel, M., Clough, S., Brown, P., Rinsland, C., Gunson, M., and Beer, R.: Tropospheric emission spectrometer: Retrieval method and error analysis, *IEEE T. Geosci. Remote*, 44, 1297–1307, 2006.
- Brasseur, G. P., Hauglustaine, D. A., Walters, S., Rasch, P. J., Müller, J.-F., Granier, C., and Tie, X. X.: MOZART, a global chemical transport model for ozone and related chemical tracers: 1. Model description, *J. Geophys. Res.*, 103, 28265–28289, <https://doi.org/10.1029/98JD02397>, 1998.
- Buchholz, R. R., Hammerling, D., Worden, H. M., Deeter, M. N., Emmons, L. K., Edwards, D. P., and Monks, S. A.: Links between carbon monoxide and climate indices for the Southern Hemisphere and tropical fire regions, *J. Geophys. Res.-Atmos.*, 123, 9786–9800, <https://doi.org/10.1029/2018JD028438>, 2018.
- Buchholz, R. R., Worden, H. M., Park, M., Francis, G., Deeter, M. N., Edwards, D. P., Emmons, L. K., Gaubert, B., Gille, J., Martínez-Alonso, S., Tang, W., Kumar, R., Drummond, J. R., Clerbaux, C., George, M. Coheur, P.-F., Hurtmans, D., Bowman, K. W., Luo, M., Payne, V. H., Worden, J. R., Chin, M., Levy, R. C., Warner, J., Wei, Z., and Kulawik, S. S.: Air pollution trends measured from Terra: CO and AOD over industrial, fire-prone, and background regions, *Remote Sens. Environ.*, 256, 112275, <https://doi.org/10.1016/j.rse.2020.112275>, 2021.
- Clerbaux, C., Hadji-Lazaro, J., Payan, S., Camy-Peyret, C., Wang, J., Edwards, D. P., and Luo, M.: Retrieval of CO from nadir remote-sensing measurements in the infrared using four different inversion algorithms, *Appl. Optics*, 41, 7068–7078, 2002.
- Clerbaux, C., Boynard, A., Clarisse, L., George, M., Hadji-Lazaro, J., Herbin, H., Hurtmans, D., Pommier, M., Razavi, A., Turquety, S., Wespes, C., and Coheur, P.-F.: Monitoring of atmospheric composition using the thermal infrared IASI/MetOp sounder, *Atmos. Chem. Phys.*, 9, 6041–6054, <https://doi.org/10.5194/acp-9-6041-2009>, 2009.
- Deeter, M., Francis, G., Gille, J., Mao, D., Martínez-Alonso, S., Worden, H., Ziskin, D., Drummond, J., Commane, R., Diskin, G., and McKain, K.: The MOPITT Version 9 CO product: sampling enhancements and validation, *Atmos. Meas. Tech.*, 15, 2325–2344, <https://doi.org/10.5194/amt-15-2325-2022>, 2022.
- Deeter, M. N., Edwards, D. P., Francis, G. L., Gille, J. C., Mao, D., Martínez-Alonso, S., Worden, H. M., Ziskin, D., and Andreae, M. O.: Radiance-based retrieval bias mitigation for the MOPITT

- instrument: the version 8 product, *Atmos. Meas. Tech.*, 12, 4561–4580, <https://doi.org/10.5194/amt-12-4561-2019>, 2019.
- Drummond, J. R., Zou, J., Nichitiu, F., Kar, J., Deschambaut, R., and Hackett, J.: A review of 9-year performance and operation of the MOPITT instrument, *Adv. Space Res.*, 45, 760774, <https://doi.org/10.1016/j.asr.2009.11.019>, 2010.
- Eyring, V., Bony, S., Meehl, G. A., Senior, C. A., Stevens, B., Stouffer, R. J., and Taylor, K. E.: Overview of the Coupled Model Intercomparison Project Phase 6 (CMIP6) experimental design and organization, *Geosci. Model Dev.*, 9, 1937–1958, <https://doi.org/10.5194/gmd-9-1937-2016>, 2016.
- Field, R. D., Luo, M., Kim, D., Del Genio, A. D., Voulgarakis, A., and Worden, J.: Sensitivity of simulated tropospheric CO to subgrid physics parameterization: A case study of Indonesian biomass burning emissions in 2006, *J. Geophys. Res.-Atmos.*, 120, 11743–11759, <https://doi.org/10.1002/2015JD023402>, 2015.
- Field, R. D., Luo, M., Fromm, M., Voulgarakis, A., Mangen, S., and Worden, J.: Simulating the Black Saturday 2009 smoke plume with an interactive composition-climate model: Sensitivity to emissions amount, timing, and injection height, *J. Geophys. Res.-Atmos.*, 121, 4296–4316, <https://doi.org/10.1002/2015JD024343>, 2016.
- Field, R. D., Luo, M., Bauer, S. E., Hickman, J. E., Elsaesser, G. S., Mezuman, K., van Lier-Walqui, M., Tsigaridis, K., and Wu, J.: Estimating the impact of a 2017 smoke plume on surface climate over northern Canada with a climate model, satellite retrievals, and weather forecasts, *J. Geophys. Res.-Atmos.*, accepted, available at ESS Open Archive, <https://doi.org/10.22541/essoar.168626418.86882614/v1>, 2023.
- Fu, D., Bowman, K. W., Worden, H. M., Natraj, V., Worden, J. R., Yu, S., Veefkind, P., Aben, I., Landgraf, J., Strow, L., and Han, Y.: High-resolution tropospheric carbon monoxide profiles retrieved from CrIS and TROPOMI, *Atmos. Meas. Tech.*, 9, 2567–2579, <https://doi.org/10.5194/amt-9-2567-2016>, 2016.
- Fu, D., Kulawik, S. S., Miyazaki, K., Bowman, K. W., Worden, J. R., Eldering, A., Livesey, N. J., Teixeira, J., Irion, F. W., Herman, R. L., Osterman, G. B., Liu, X., Levelt, P. F., Thompson, A. M., and Luo, M.: Retrievals of tropospheric ozone profiles from the synergism of AIRS and OMI: methodology and validation, *Atmos. Meas. Tech.*, 11, 5587–5605, <https://doi.org/10.5194/amt-11-5587-2018>, 2018.
- Fu, D., Millet, D. B., Wells, K. C., Payne, V. H., Yu, S., Guenther, A., and Eldering, A.: Direct retrieval of isoprene from satellite based infrared measurements, *Nat. Commun.*, 10, 3811, <https://doi.org/10.1038/s41467-019-11835-0>, 2019.
- Gambacorta, A. and Barnet, C. D.: Methodology and Information Content of the NOAA NESDIS Operational Channel Selection for the Cross-Track Infrared Sounder (CrIS), *IEEE T. Geosci. Remote.*, 51, 3207–3216, <https://doi.org/10.1109/TGRS.2012.2220369>, 2013.
- Gambacorta, A., Barnet, C., Wolf, W., King, T., Maddy, E., Strow, L., Xiong, X., Nalli, N., and Goldberg, M.: An Experiment Using High Spectral Resolution CrIS Measurements for Atmospheric Trace Gases: Carbon Monoxide Retrieval Impact Study, *IEEE Geosci. Remote Sens. Lett.*, 11, 1639–1643, <https://doi.org/10.1109/LGRS.2014.2303641>, 2014.
- George, M., Clerbaux, C., Hurtmans, D., Turquety, S., Coheur, P.-F., Pommier, M., Hadji-Lazaro, J., Edwards, D. P., Worden, H., Luo, M., Rinsland, C., and McMillan, W.: Carbon monoxide distributions from the IASI/METOP mission: evaluation with other space-borne remote sensors, *Atmos. Chem. Phys.*, 9, 8317–8330, <https://doi.org/10.5194/acp-9-8317-2009>, 2009.
- George, M., Clerbaux, C., Bouarar, I., Coheur, P.-F., Deeter, M. N., Edwards, D. P., Francis, G., Gille, J. C., Hadji-Lazaro, J., Hurtmans, D., Inness, A., Mao, D., and Worden, H. M.: An examination of the long-term CO records from MOPITT and IASI: comparison of retrieval methodology, *Atmos. Meas. Tech.*, 8, 4313–4328, <https://doi.org/10.5194/amt-8-4313-2015>, 2015.
- Han, Y., Revercomb, H., Cromp, M., Gu, D., Johnson, D., Mooney, D., Scott, D., Strow, L., Bingham, G., Borg, L., Chen, Y., DeSlover, D., Esplin, M., Hagan, D., Jin, X., Knuteson, R., Motteler, H., Predina, J., Suwinski, L., Taylor, J., Tobin, D., Tremblay, D., Wang, Ch., Wang, L., Wang, L., and Zavyalov, V.: Suomi NPP CrIS measurements, sensor data record algorithm, calibration and validation activities, and record data quality, *J. Geophys. Res.-Atmos.*, 118, 12734–12784, <https://doi.org/10.1002/2013JD020344>, 2013.
- Hegarty, J. D., Cady-Pereira, K. E., Payne, V. H., Kulawik, S. S., Worden, J. R., Kantchev, V., Worden, H. M., McKain, K., Pittman, J. V., Commane, R., Daube Jr., B. C., and Kort, E. A.: Validation and error estimation of AIRS MUSES CO profiles with HIPPO, ATom, and NOAA GML aircraft observations, *Atmos. Meas. Tech.*, 15, 205–223, <https://doi.org/10.5194/amt-15-205-2022>, 2022.
- Hoesly, R. M., Smith, S. J., Feng, L., Klimont, Z., Janssens-Maenhout, G., Pitkanen, T., Seibert, J. J., Vu, L., Andres, R. J., Bolt, R. M., Bond, T. C., Dawidowski, L., Kholod, N., Kurokawa, J.-I., Li, M., Liu, L., Lu, Z., Moura, M. C. P., O'Rourke, P. R., and Zhang, Q.: Historical (1750–2014) anthropogenic emissions of reactive gases and aerosols from the Community Emissions Data System (CEDS), *Geosci. Model Dev.*, 11, 369–408, <https://doi.org/10.5194/gmd-11-369-2018>, 2018.
- Jacob, D.: *Introduction to Atmospheric Chemistry*, Princeton University Press, ISBN 9780691001852, 1999.
- Kaiser, J. W., Heil, A., Andreae, M. O., Benedetti, A., Chubarova, N., Jones, L., Morcrette, J.-J., Razinger, M., Schultz, M. G., Suttie, M., and van der Werf, G. R.: Biomass burning emissions estimated with a global fire assimilation system based on observed fire radiative power, *Biogeosciences*, 9, 527–554, <https://doi.org/10.5194/bg-9-527-2012>, 2012.
- Kalnay, E., Kanamitsu, M., Kistler, R., Collins, W., Deaven, D., Gandin, L., Iredell, M., Saha, S., White, G., Woollen, J., Zhu, Y., Chelliah, M., Ebisuzaki, W., Higgins, W., Janowiak, J., Mo, K. C., Ropelewski, C., Wang, J., Leetmaa, A., Reynolds, R., Jenne, R., and Joseph, D.: The NCEP/NCAR 40-year reanalysis project, *B. Am. Meteorol. Soc.*, 77, 437–471, [https://doi.org/10.1175/1520-0477\(1996\)077<0437:tnyrp>2.0.co;2](https://doi.org/10.1175/1520-0477(1996)077<0437:tnyrp>2.0.co;2), 1996.
- Kelley, M., Schmidt, G. A., Nazarenko, L. S., Bauer, S. E., Ruedy, R., Russell, G. L., Ackerman, A. S., Aleinov, I., Bauer, M., Bleck, R., Canuto, V., Cesana, G., Cheng, Y., Clune, T. L., Cook, B. I., Cruz, C. A., Del Genio, A. D., Elsaesser, G. S., Faluvegi, G., Kiang, N. Y., Kim, D., Lacis, A. A., Leboissetier, A., LeGrande, A. N., Lo, K. K., Marshall, J., Matthews, E. E., McDermid, S., Mezuman, K., Miller, R. L., Murray, L. T., Oinas, V., Orbe, C., García-Pando, C. P., Perlwitz, J. P., Puma, M. J., Rind, D., Romanou, A., Shindell, D. T., Sun, S., Tausnev, N., Tsigaridis, K,

- Tselioudis, D., Weng, E., Wu, J., and Yao, M.-S.: GISS-E2.1: Configurations and Climatology, *J. Adv. Model. Earth Syst.*, 12, e2019MS002025, <https://doi.org/10.1029/2019ms002025>, 2020.
- Kulawik, S. S., Bowman, K. W., Luo, M., Rodgers, C. D., and Jourdain, L.: Impact of nonlinearity on changing the a priori of trace gas profile estimates from the Tropospheric Emission Spectrometer (TES), *Atmos. Chem. Phys.*, 8, 3081–3092, <https://doi.org/10.5194/acp-8-3081-2008>, 2008.
- Lamarque, J.-F., Emmons, L. K., Hess, P. G., Kinnison, D. E., Tilmes, S., Vitt, F., Heald, C. L., Holland, E. A., Lauritzen, P. H., Neu, J., Orlando, J. J., Rasch, P. J., and Tyndall, G. K.: CAM-chem: description and evaluation of interactive atmospheric chemistry in the Community Earth System Model, *Geosci. Model Dev.*, 5, 369–411, <https://doi.org/10.5194/gmd-5-369-2012>, 2012.
- Lassman, W., Mirocha, J. D., Arthur, R. S., Kochanski, A. K., Farguella Caus, A., Bagley, A. M., Carreras Sospedra, M., Dabdub, D., and Barbato, M.: Using satellite-derived fire arrival times for coupled wildfire-air quality simulations at regional scales of the 2020 California wildfire season, *J. Geophys. Res.-Atmos.*, 128, e2022JD037062, <https://doi.org/10.1029/2022JD037062>, 2023.
- Liu, J., Logan, J. A., Jones, D. B. A., Livesey, N. J., Megretskiaia, I., Carouge, C., and Nedelec, P.: Analysis of CO in the tropical troposphere using Aura satellite data and the GEOS-Chem model: insights into transport characteristics of the GEOS meteorological products, *Atmos. Chem. Phys.*, 10, 12207–12232, <https://doi.org/10.5194/acp-10-12207-2010>, 2010.
- Luo, M., Rinsland, C., Fisher, B., Sachse, G., Diskin, G., Logan, J., Worden, H., Kulawik, S., Osterman, G., Eldering, A., Herman, R., and Shephard, M.: TES carbon monoxide validation with DACOM aircraft measurements during INTEX-B 2006, *J. Geophys. Res.*, 112, D24S48, <https://doi.org/10.1029/2007JD008803>, 2007a.
- Luo, M., Rinsland, C. P., Rodgers, C. D., Logan, J. A., Worden, H., Kulawik, S., Eldering, A., Goldman, A., Shephard, M. W., Gunson, M., and Lampel, M.: Comparison of carbon monoxide measurements by TES and MOPITT: Influence of a priori data and instrument characteristics on nadir atmospheric species retrievals, *J. Geophys. Res.*, 112, D09303, <https://doi.org/10.1029/2006JD007663>, 2007b.
- NASA/LARC/SD/ASDC: MOPITT Derived CO (Thermal Infrared Radiances) V009, NASA Langley Atmospheric Science Data Center DAAC [data set], <https://doi.org/10.5067/TERRA/MOPITT/MOP02T.009>, 2024.
- Noël, S., Reuter, M., Buchwitz, M., Borchardt, J., Hilker, M., Schneising, O., Bovensmann, H., Burrows, J. P., Di Noia, A., Parker, R. J., Suto, H., Yoshida, Y., Buschmann, M., Deutscher, N. M., Feist, D. G., Griffith, D. W. T., Hase, F., Kivi, R., Liu, C., Morino, I., Notholt, J., Oh, Y.-S., Ohyama, H., Petri, C., Pollard, D. F., Rettinger, M., Roehl, C., Rousogonous, C., Sha, M. K., Shiomi, K., Strong, K., Sussmann, R., Té, Y., Velasco, V. A., Vrekoussis, M., and Warneke, T.: Retrieval of greenhouse gases from GOSAT and GOSAT-2 using the FOCAL algorithm, *Atmos. Meas. Tech.*, 15, 3401–3437, <https://doi.org/10.5194/amt-15-3401-2022>, 2022.
- Rémy, S., Veira, A., Paugam, R., Sofiev, M., Kaiser, J. W., Marengo, F., Burton, S. P., Benedetti, A., Engelen, R. J., Ferrare, R., and Hair, J. W.: Two global data sets of daily fire emission injection heights since 2003, *Atmos. Chem. Phys.*, 17, 2921–2942, <https://doi.org/10.5194/acp-17-2921-2017>, 2017.
- Rodgers, C. D.: Inverse Methods for Atmospheric Sounding: Theory and Practice, World Scientific, Singapore, ISBN 981-02-2740-X, 2000.
- Smith, N. and Barnett, C. D.: CLIMCAPS observing capability for temperature, moisture, and trace gases from AIRS/AMSU and CrIS/ATMS, *Atmos. Meas. Tech.*, 13, 4437–4459, <https://doi.org/10.5194/amt-13-4437-2020>, 2020.
- Strode, S. A., Worden, H. M., Damon, M., Douglass, A. R., Duncan, B. N., Emmons, L. K., Lamarque, J.-F., Manyin, M., Oman, L. D., Rodriguez, J. M., Strahan, S. E., and Tilmes, S.: Interpreting space-based trends in carbon monoxide with multiple models, *Atmos. Chem. Phys.*, 16, 7285–7294, <https://doi.org/10.5194/acp-16-7285-2016>, 2016.
- Tilmes, S., Lamarque, J.-F., Emmons, L. K., Kinnison, D. E., Marsh, D., Garcia, R. R., Smith, A. K., Neely, R. R., Conley, A., Vitt, F., Val Martin, M., Tanimoto, H., Simpson, I., Blake, D. R., and Blake, N.: Representation of the Community Earth System Model (CESM1) CAM4-chem within the Chemistry-Climate Model Initiative (CCMI), *Geosci. Model Dev.*, 9, 1853–1890, <https://doi.org/10.5194/gmd-9-1853-2016>, 2016.
- Veefkind, J. P., Aben, I., McMullan, K., Forster, H., de Vries, J., Otter, G., Claas, J., Eskes, H. J., de Haan, J. F., Kleipool, Q., van Weele, M., Hasekamp, O., Hoogeveen, R., Landgraf, J., Snel, R., Tol, P., Ingmann, P., Voors, R., Kruizinge, B., Vink, R., Visser, H., and Levelt, P. F.: TROPOMI on the ESA Sentinel-5 Precursor: A GMES mission for global observations of the atmospheric composition for climate, air quality and ozone layer applications, *Remote Sens. Environ.*, 120, 70–83, 2012.
- Worden, H. M., Logan, J. A., Worden, J. R., Beer, R., Bowman, K., Clough, S. A., Eldering, A., Fisher, B. M., Gunson, M. R., Herman, R. L., Kulawik, S. S., Lampel, M. C., Luo, M., Megretskiaia, I. A., Osterman, G. B., and Shephard, M. W.: Comparisons of Tropospheric Emission Spectrometer (TES) ozone profiles to ozonesondes: Methods and initial results, *J. Geophys. Res.*, 112, D03309, <https://doi.org/10.1029/2006JD007258>, 2007.
- Worden, H. M., Deeter, M. N., Frankenberg, C., George, M., Nichitiu, F., Worden, J., Aben, I., Bowman, K. W., Clerbaux, C., Coheur, P. F., de Laat, A. T. J., Detweiler, R., Drummond, J. R., Edwards, D. P., Gille, J. C., Hurtmans, D., Luo, M., Martínez-Alonso, S., Massie, S., Pfister, G., and Warner, J. X.: Decadal record of satellite carbon monoxide observations, *Atmos. Chem. Phys.*, 13, 837–850, <https://doi.org/10.5194/acp-13-837-2013>, 2013.
- Worden, H. M., Francis, G. L., Kulawik, S. S., Bowman, K. W., Cady-Pereira, K., Fu, D., Hegarty, J. D., Kantchev, V., Luo, M., Payne, V. H., Worden, J. R., Commane, R., and McKain, K.: TROPES/CrIS carbon monoxide profile validation with NOAA GML and ATom in situ aircraft observations, *Atmos. Meas. Tech.*, 15, 5383–5398, <https://doi.org/10.5194/amt-15-5383-2022>, 2022.
- Zeng, Z.-C., Lee, L., and Qi, C.: Diurnal carbon monoxide observed from a geostationary infrared hyperspectral sounder: first result from GIIRS on board FengYun-4B, *Atmos. Meas. Tech.*, 16, 3059–3083, <https://doi.org/10.5194/amt-16-3059-2023>, 2023.